Mitigation of the refraction error in surveying techniques by using a network of meteorological sensors and a 3D refractivity model

Luis GARCÍA-ASENJO[1,*], **Raquel LUJÁN**[1], and **Sergio BASELGA**[1]

[1] *Department of Cartographic Engineering, Geodesy and Photogrammetry, Universitat Politècnica de València, Valencia, Spain,(lugarcia@cgf.upv.es, ralugar@cgf.upv.es, serbamo@cgf.upv.es)*

[*] *corresponding author*

Abstract

Different geomatic techniques and instruments can be used for deformation monitoring from a nearby control network, including electro-optical distance meters (EDM), terrestrial laser scanners (TLS), total stations (TS), and Global Navigation Satellite Systems (GNSS). However, atmospheric refraction can largely diminish the attainable accuracy of angle and distance measurements especially in long ranges, that is, those from few hundred meters to several kilometers, thus hampering the proper integration of the measurements into a high-accuracy reference frame and the subsequent reliable determination of possible displacements. This work describes the approach used in a long-term deformation monitoring project in Cortes de Pallás (Spain), where a network of meteorological sensors was deployed in selected points and subsequently used to build a 3D refractivity model. The consistency of the model is verified by using a robotic TS and well-known coordinates, and then applied to long-range TLS data. The results show that a few meteorological sensors well distributed in selected points of the area can mitigate the refraction error better than the traditional approach based on only measuring the meteorological parameters at the station and, when it is feasible, at the target point.

Keywords: atmospheric refraction, EDM, TS, TLS, meteorological sensors

1 Introduction

Deformation monitoring by using surveying techniques such as electro-optical distance measurements (EDM), total station measurements (TS), or terrestrial laser scanning (TLS) is affected by atmospheric refraction in several ways. Firstly, refraction limits the nominal accuracy of the used instruments by introducing systematic scale or angular errors (Brunner, 1984; Ingesand, 2008; Baselga et al., 2014). Secondly, the subsequent nonhomogenous propagation of those errors to coordinates hampers the rigorous co-registration into a unique reference frame. Thirdly, even when high-precision measurements are used to establish or monitor high-precision reference frames, residual refraction can introduce scale and orientation distortions in the own reference frame, thus leading to wrong conclusions with regard to the stability of the reference system, which is a critical aspect for the rigorous assessment of possible displacements overtime (Niemeier, 1981; Caspary, 1987; García-Asenjo et al., 2023).

Given the importance of the problem, new instruments and methodologies are being developed to eliminate refraction in distances, such as high-precision two-wavelength distance meters (Guillory et al., 2023; Ray et al., 2023) or the use of GNSS as a high-accuracy distance meter (García-Asenjo et al., 2021; Baselga et al., 2022). However, these innovative approaches, which are primarily used in fields such as length metrology, are still under development, and therefore, the need to apply atmospheric corrections in terrestrial geodetic techniques by means of external meteorological data still remains.

The traditional approach to mitigate atmospheric refraction involves estimating either the index of refraction or its vertical gradient from empirical equations based on meteorological parameters measured at both ends of the baseline (IAG, 1999). This approach, which is specially cumbersome when using analogic thermometers and barometers, is not even possible in monitoring works where the target points are not accesible or when operational lim-

itations make it difficult the use of sensors in all stations. Moreover, this traditional approach has proven insufficient due to the inadequate representation of the atmospheric conditions along the entire path specially in complex terrains where the atmospheric conditions can vary significantly along the path (Rüeger, 1992; Neyezhmakov and Prokopov, 2022).

To overcome the aforementioned problem, we propose the use of a 3D refractivity model (3D-RM) that integrates in-situ meteorological data from a network of automatic data-loggers, terrain information from a digital terrain model (DTM), and sensible heat flux from ERA5 (Martens et al., 2020; Muñoz Sabater et al., 2021). A similar approach can be found in Kerekes (2023), although only applied to a theoretical estimation of TLS measurement errors. In particular, our model implements the Turbulence Transfer Model (TTM) as presented in Dodson and Zaher (1985), which provides equations for deriving refractivity gradients from parameters measured in the field (i.e.air temperature, pressure, humidity, heat flux, and wind speed). That is, classical concepts as TTM are revisited by taking advantage of automatic atmospheric sensors, which can be adquired at a relatively low cost, and the availability of new global remote sensing products, so that a refractivity correction model is build for automatic processing.

Since meteorological data-loggers, which automatically collect the temperature, humidity and pressure of the air, are usually limited to a certain number, two versions of the refractivity model are tested. The first version (3D-RM) incorporates meteorological data from all the installed sensors, including the station point, while the second version (3D-RM 2) excludes the station sensor, estimating its value from the remaining sensors of the network. Anyway, the main research question to be addressed is how the atmospheric effects in distances and angles can be characterized from a discrete number of stationary meteorological sensors.

Section 2 summarizes the main aspects of the proposed refractivity model. The model has been tested in two different field experiments that are described in Section 3 Their results are analyzed and discussed in Section 4 Finally, some conclusions and future work are summarized in Section 5

2 3D refractivity model

The difficulty of properly modeling the atmospheric effects in distances and angles lies in the complexity of the physical processes in the lowest part of the atmosphere, where there is significant interaction between the ground and the atmosphere. Extensive studies on these processes have been made since the 1950s (Obukhov, 1949; Priestley, 1949; Brunner, 1984).

Our proposed model (3D-RM), which is thoroughly described in Luján et al. (2025), is based on two key principles: vertical layering and spatial interpolation. Firstly, the TTM as described in Dodson and Zaher (1985) is applied on each meteorological station for vertical characterization of both refractivity values and gradients. Secondly, the refractivity information obtained is used to perform spatial interpolation at specific heights. These values are subsequently integrated for each baseline measured. Figure 1 illustrates the basis of the model with these two fundamental ideas.

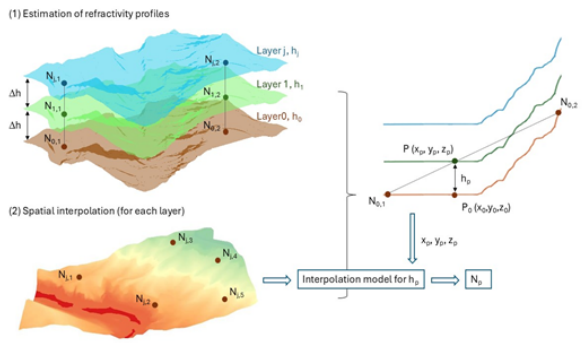

Figure 1. Model basis: (1) Estimation of refractivity profiles or layering, (2) Spatial interpolation for each layer.

Meteorological sensors are deployed at specific locations within the study area, each installed at a height above ground ($h_{0,i}$), where i represents each meteorological sensor. The sensors are assumed to be positioned at approximately the same height, denoted as h_0. If it is not the case, that is, when sensors are installed at significantly different heights above ground (i.e. with differences exceeding the chosen interval between layers, h), the TTM is used to refer the refractivity values to a common reference height above ground h_0.

At each meteorological station i, the refractivity at

the reference height h_0 (denoted $N_{0,i}$) is calculated using local meteorological parameters. Since the interaction between the Earth's surface and the lower atmosphere decreases with height, the atmosphere is divided into layers that are approximately parallel to the DTM surface at discrete heights above ground level, 1 m for instance. The vertical refractivity gradient is then estimated for each layer by applying the TTM, which is subsequently used to propagate the refractivity from the lower layer to the upper ones, resulting in a set of refractivity values for discrete vertical layers at each meteorological station. For each particular layer, a spatial interpolation is performed to estimate the refractivity at any point P inside the study area at this specific height, so that an interpolation model is constructed for each layer.

The model implementation is divided into 4 steps: estimation of refractivity profiles, spatial interpolation at each layer, model application to observations, and calculation of distance and vertical angle corrections. The overall workflow of the model is shown in Figure 2.

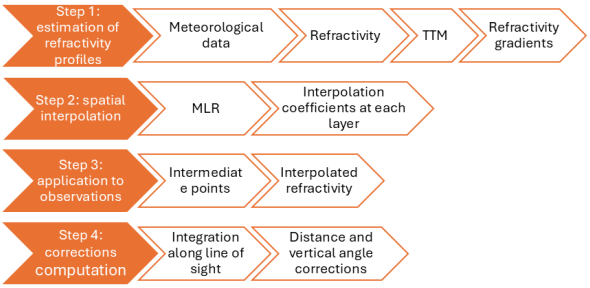

Figure 2. Workflow to build the 3D-RM.

Since this study also seeks to know the capabilities and possible limitations of the model, it was deemed necessary to test two versions of the model. The first version (3D-RM) uses the meteorological data from sensors installed in all the station points, while the second version (3D-RM 2) does not use the station sensor, thus estimating the reafractivity value from the remaining sensors of the network. This second version enables the use of the model with a limited number of sensors which can be statically located in those points that better characterize the local atmosphere instead of moving them to the measuring stations.

3 Experimental validation

The area selected for the assessment of the proposed 3D refractivity model was La Muela in Cortes de Pallás (Spain), where the Diputació de València and the Universitat Politècnica de València (UPV) collaborate on a long-term deformation monitoring project since 2017.

Among the reasons that explain why this area perfectly suits the purpose of this study, we can highlight the complex topography and the existence of a well-controlled geodetic network of ten pillars in the area along with the 15 reflector prisms permanently located on the cliff that can be used as control points (CPs).

The complex topography, which includes a cliff and a water reservoir, prevents the installation of meteorological sensors at the CPs (García-Asenjo et al., 2019).

Figure 3. Pillar 8006 equipped with a ⌀0.5 m target sphere and a meteorological data logger used to eliminate the refraction error. Pillar 8009, which was used as TLS station in 2023 and TS station in 2024, is marked in red. The sunshade was removed for taking the pictures.

Since the geodetic network and the CPs have been periodically measured using high-precision methodology with a sub-millimetric EDM Kern Mekometer ME5000, the accuracy of the coordinates for the geodetic pillars is better than 1 mm and 3 mm in the horizontal and vertical components, respectively, while the accuracy for the CPs is slightly lower due to the measurement geometry, the type

of prism used, and the fact that no meteorological sensor can be installed on the cliff (García-Asenjo et al., 2023). In this study, the coordinates of pillars and CPs will be used as ground-truth to calculate theoretical distances and angles.

Two campaigns were performed to test the model. The first campaign took place on July 20, 2023, and was focused on obtaining the initial results of the model. During this campaign, 10 data-loggers were installed (see Fig. 5), 5 TS series were hourly taken from 8 AM to 11 AM. Additionally, 6 long-range TLS sets of measurements were collected from pillars 8002 and 8009. For point cloud registration, five pillars (8003, 8004, 8005, 8006, and 8011) of the geodetic network were equipped with a ⌀0.5 m target sphere (see Figure 3).

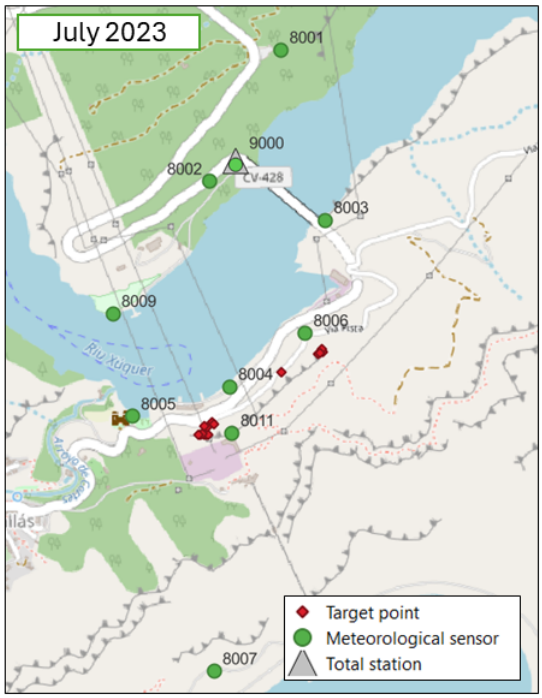

Figure 4. Locations of the involved points for the first campaign (July 2023). During this campaign, 10 meteo data-loggers were used, and both TS and TLS measurements were collected.

The second campaign, carried out on June 25, 2024, was planned to cover a broader time range to better analyze the effects of refraction from sun-rise to sunset, and only 7 meteorological data-loggers were deployed (see Fig. 5). In this campaign, 5 TS series were automatically recorded hourly from station 8009 from approximately 7 AM to 10 PM.

In 2023, the TS, a Leica TM30 robotic total station,

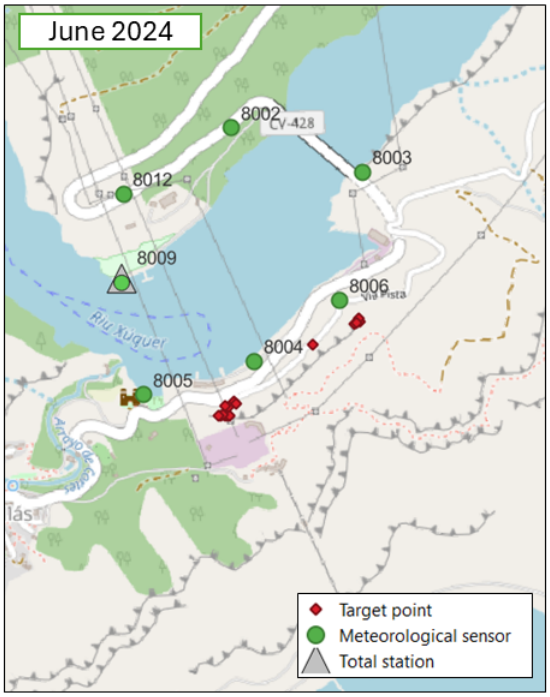

Figure 5. Locations of the involved points for the second campaign (June 2024). During this campaign, 7 meteo data-loggers were used, and only TS measurements were collected.

was mounted on a tripod over a permanent benchmark (named 9000) while in 2024, the same total station was set up on one pillar of the geodetic network (point 8009). In both campaigns, the measurement series were recorded automatically, using dual-face observations. This type of experiment requires samples large enough to be considered statistically significant, which necessarily involves the use of automatic measuring systems. At this point, it is worth noting that vertical angles collected by using an automated target recognition system (ATR) and internal algorithms can conceal the influence of refraction. Moreover, current TSs cannot easily isolate vertical refraction from other potential sources of error such as vertical deflection or limitations in the vertical compensator.

Regarding meteorological sensors, we used Testo 176P1 data-loggers equipped with temperature and humidity probes previously calibrated at the UPV calibration laboratory. The results of the calibration showed that their accuracy under laboratory conditions was ± 0.2 K and ± 1.8 hPa for temperature and air pressure respectively. During the field campaigns, they were installed within self-ventilated

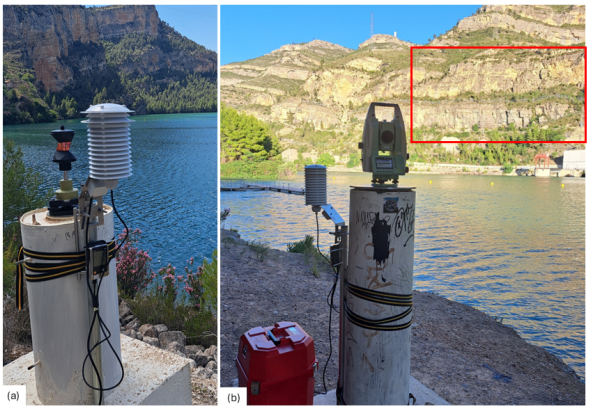

Figure 6. (a) Detail of a meteorological sensor with self-ventilated shelter. (b) Total station and meteorological sensor in pillar 8009 in the June 2024 campaign. The area of target points is marked in red. Sunshades were removed for taking the pictures.

shelters firmly attached to the selected pillars of the geodetic network and additionally protected with a sunshade (see Figure 6). The meteorological sensors (10 in 2023, and only 7 in 2024) were programmed to automatically record temperature, humidity, and air pressure at 60 s intervals, which is considered optimal for efficient modeling of the local meteorological conditions.

4 Results and discussion

The experiments were designed to assess the model performance in terms of precision (repeatability under similar conditions), and accuracy (reproducibility under different conditions). To assess the model precision, the standard deviations are analyzed, while proximity to reference values derived from the known coordinates of pillars and CPs is used to evaluate its accuracy. The model's performance is also compared against the standard correction method. Similarly to many real deformation monitoring projects with non-accesible target points, in this case, the standard method only uses meteorological data collected at the station.

For distance measurements, the refraction corrections obtained in the first campaign (with distances around 800 m) are of the order of 2 cm, while the second campaign (with distances around 450 m) yielded corrections of the order of 1 cm. These corrections from the 3D-RM were generally slightly higher than those from the standard approach by using meteorological data only at the station point. In terms of standard deviation, while the improvements relative to the standard method were not always significant, the values obtained still met the precision of the instrument. As an illustration, Figure 7 shows the variation in measured distances and the correction obtained using the 3D-RM in CP No.7 in both campaigns (2023 and 2024).

When it comes to accuracy, defined as closeness to reference values, a general improvement of around 2 mm was observed in the July 2023 campaign when using the 3D-RM compared to the standard approach. In the June 2024 campaign, results proved less significative, with improvements at only some target points. Even so, the differences compared to the standard approach were not significant. Additionally, 3D-RM2 delivered almost identical results to the original 3D-RM model, which reinforces the practicality and effectiveness of the method.

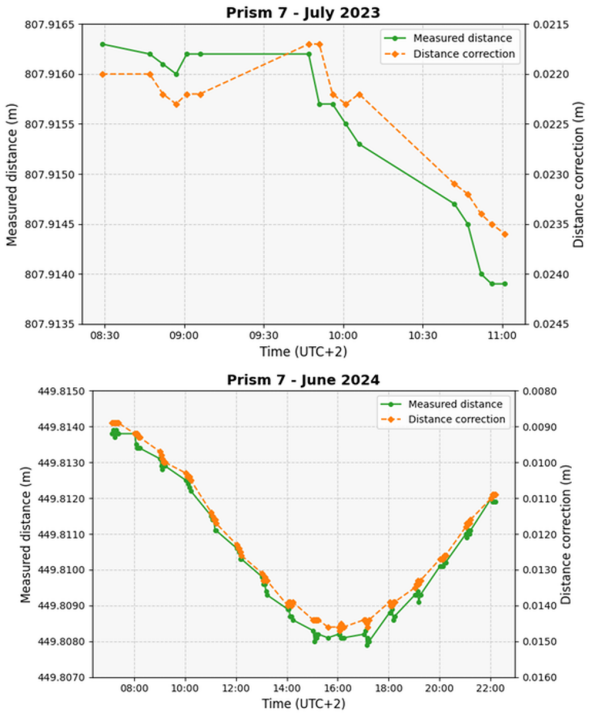

Figure 7. Evolution of the measured distances and the corresponding corrections for CP No.7, in July 2023 and June 2024, respectively.

Concerning vertical angles, Table 1 presents the general results obtained in year 2023 from the 9000 station, including the average vertical angle for every line of sight, the average correction, the standard deviation of the measured angle, and the standard

deviation of the corrected angle.

Table 1. Vertical angles results from point 9000 to all the observed points. Includes the measured vertical angle (VA_m, in gons), the mean correction obtained (Corr, in mgons), the standard deviation of both the measured (σ_{VA_m}, in mgons) and corrected angles (σ_{VA_c}, in mgons).

Point	VA_m	**Corr**	σ_{VA_m}	σ_{VA_c}
1	92.01582	0.07	0.23	0.22
2	92.38039	0.07	0.28	0.21
3	91.91924	0.07	0.23	0.25
4	93.99555	0.06	0.35	0.29
5	94.30574	0.06	0.23	0.26
6	94.52214	0.06	0.28	0.16
7	96.37246	0.04	0.21	0.20
8	97.45429	0.01	0.27	0.25
9	96.36063	0.02	0.28	0.21
10	95.56458	-0.08	0.29	0.17
11	90.13404	-0.08	0.36	0.22
12	88.16614	-0.08	0.36	0.22
13	89.72186	-0.09	0.42	0.27
14	88.41129	-0.09	0.43	0.28
15	96.76641	0.02	0.21	0.23

The 3D-RF was also applied to the TLS measurements collected in year 2023. For the sake of conciseness, only graphic results for one point cloud are shown in Figures 8 and 9.

Figure 8 shows the differences between the original point cloud with refraction and the same point cloud corrected from refraction by using the proposed 3D-RM. Taking into account that this study requires the TLS data to be rigorously integrated into the existing high-precision reference frame with no scale modification, the registration process was performed by using a dedicate transformation with only three rotational parameters and the station coordinates assumed to be known. Otherwise, the classical registration would absorb part of the refraction and would also change the line of sight direction of every collected point. The differences found ranged from 1.7 cm to 7.0 cm.

Figure 9 shows the differences between the point cloud with the original registration and the point cloud registered with the CP coordinates corrected from refraction. The differences found ranged in this case from 1.5 cm to 5.6 cm.

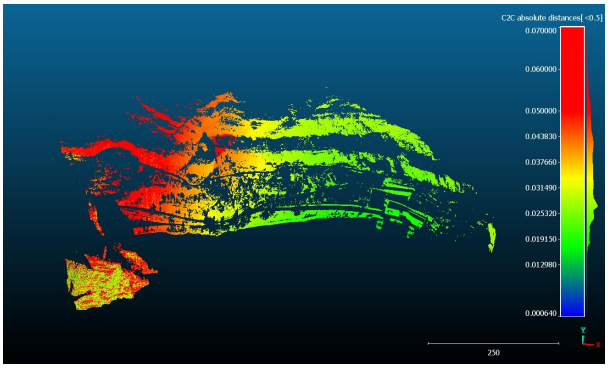

Figure 8. Differences between the original point cloud with refraction and the same point cloud corrected from refraction by using the proposed 3D-RM (July 2023)

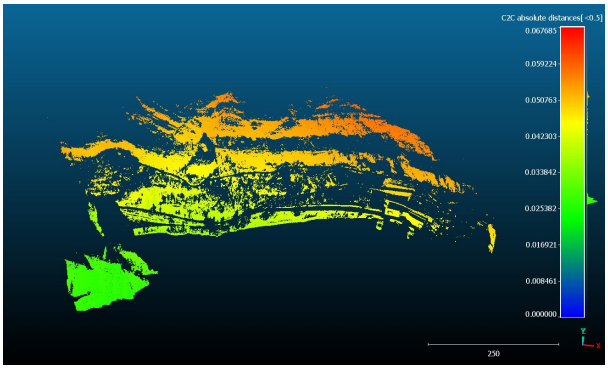

Figure 9. Differences between the point cloud with the original registration and the point cloud registered with the CP coordinates corrected from refraction (July 2023)

5 Conclusions and future work

This paper introduces the 3D refractivity model (3D-RM), which is based on current low-cost automatic atmospheric sensors and publicly available data products to estimate refractivity and refractivity gradients at every point within a working area to provide a refractivity correction suitable for automatic processing.

The proposed 3D-RM performed well in the two field experiments, providing reliable corrections even when no meteorological data were available at the target points. The second version of the model (3D-RM 2), which estimates corrections without using the sensor at the measuring station, produced nearly identical results to the full sensor-based model. This feature makes the model highly adaptable because the sensors can be better located

in those points that better characterize the local refraction, which do not necessarily coincide with the measuring stations. By reducing the number of required sensors just to cover the area of interest, the model enables rapid and cost-effective measurements without the need to relocate sensors, significantly reducing setup time and operational costs.

The use of ERA5 data for estimating sensible heat flux proved to be a valuable component in the vertical layering of the model. This integration allowed for accurate vertical refractivity profiles within the boundary layer, without increasing the costs of the processing and the field campaigns.

The proposed model can be safely used to eliminate the refraction error from measured distances, but special care must be taken when processing vertical angles because the use of automatic ATR systems may involve automatic adjustments by the instrument's internal algorithms. Although vertical angle measurements without ATR could be considered to ensure the angles reflect the actual refractive effects, taking manual measurements would necessarily entail smaller samples.

While the model's performance is promising, there is room for future work, such as additional testing in a broader range of atmospheric conditions in order to better understand the model's robustness and limitations.

Acknowledgements

The authors are grateful to the Diputació de València, which allow the use of the geodetic infrastructure established in La Muela de Cortes de Pallás (Spain) under the contract T-726. The research contract of Raquel Luján was funded by the Programa de Ayudas de Investigación y Desarrollo (PAID-01-20) de la Universitat Politècnica de València. This work was partially funded by the project Development of High-Precision GNSS Techniques for Dimensional Metrology, Deformation Monitoring, and Geodetic Networks for Civil Engineering Projects (GNSS-Metrology), ref. PID2022-142363NB-I00, Plan Estatal de Investigación Científica y Técnica y de Innovación 2021-2023, MCIN/AEI/10.13039/501100011033/FEDER, UE.

References

Baselga, S., García-Asenjo, L., and Garrigues, P. (2014). Practical formulas for the refraction coefficient. *Journal of Surveying Engineering*, 140(2):06014001.

Baselga, S., García-Asenjo, L., Garrigues, P., and Luján, R. (2022). GBDM+: an improved methodology for a gnss-based distance meter. *Measurement Science and Technology*, 33(8):085020.

Brunner, F. K. (1984). *Geodetic Refraction: Effects of Electromagnetic Wave Propagation through the Atmosphere*. Springer-Verlag: Berlin Heidelberg.

Caspary, W. F. (1987). *Concepts of network and deformation analysis*. School of Surveying, The University of New South Wales, Australia, Monograph 11.

Dodson, A. H. and Zaher, M. (1985). Refraction effects on vertical angle measurements. *Survey Review*, 28(217):169–183.

García-Asenjo, L., Baselga, S., Atkins, C., and Garrigues, P. (2021). Development of a submillimetric GNSS-based distance meter for length metrology. *Sensors*, 21(4).

García-Asenjo, L., Martínez, L., Baselga, S., Garrigues, P., and Luján, R. (2019). Establishment of a multi-purpose 3D geodetic reference frame for deformation monitoring in Cortes de Pallás (Spain). In *Proceedings of the 4th Joint International Symposium on Deformation Monitoring (JISDM)*.

García-Asenjo, L., Martínez, L., Baselga, S., Garrigues, P., and Luján, R. (2023). Design, establishment, analysis, and quality control of a high-precision reference frame in Cortes de Pallás (spain). *Applied Geomatics*, 15(2):359–370.

Guillory, J., Truong, D., Wallerand, J.-P., and Alexandre, C. (2023). A sub-millimetre two-wavelength EDM that compensates the air refractive index: uncertainty and measurements up to 5 km. *Measurement Science and Technology*, 35(2):025024.

IAG (1999). *Resolutions Adopted at the XXIIth General Assembly*. Birmingan, International Association of Geodesy (IAG).

Ingesand, H. (2008). Concepts and solutions to overcome the refraction problem in terrestrial precision measurement. *Geodesy and Cartography*, 34:61–65.

Kerekes, G. (2023). *An elementary error model for terrestrial laser scanning*, volume Heft Nr. 900 of *DGK: C (Dissertationen)*. München.

Luján, R., García-Asenjo, L., and Baselga, S. (2025). 3D refractivity model for atmospheric mitigation in distance and vertical angle measurements. *Submitted (under-review)*.

Martens, B., Schumacher, D. L., Wouters, H., Muñoz Sabater, J., Verhoest, N. E. C., and Miralles, D. G. (2020). Evaluating the land-surface energy partitioning in era5. *Geoscientific Model Development*, 13(9):4159–4181.

Muñoz Sabater, J., Dutra, E., Agustí-Panareda, A., Albergel, C., Arduini, G., Balsamo, G., Boussetta, S., Choulga, M., Harrigan, S., Hersbach, H., Martens, B., Miralles, D. G., Piles, M., Rodríguez-Fernández, N. J., Zsoter, E., Buontempo, C., and Thépaut, J.-N. (2021). Era5-land: a state-of-the-art global reanalysis dataset for land applications. *Earth System Science Data*, 13(9):4349–4383.

Neyezhmakov, P. and Prokopov, A. (2022). On the accuracy of determining the mean integral refractive index of air by its values at the end points of the trace. In *2022 XXXII International Scientific Symposium Metrology and Metrology Assurance (MMA)*, pages 1–4.

Niemeier, W. (1981). Statistical tests for detecting movements in repeatedly measured geodetic networks. *Tectonophysics*, 71(1):335–351. Proceedings of the IUGG Interdisciplinary Symposium No. 9, "Recent Crustal Movements".

Obukhov, A. (1949). Structure of the temperature field in turbulent flow. *Izv. Akad. Nauk SSSR Ser. Geogr. Geofiz.*, 13:58–69.

Priestley, C. (1949). Turbulent transfer in the lower atmosphere. *Izv. Akad. Nauk SSSR Ser. Geogr. Geofiz.*, 13:58–69.

Ray, P., Salido-Monzú, D., and Wieser, A. (2023). High-precision intermode beating electro-optic distance measurement for mitigation of atmospheric delays. *Journal of Applied Geodesy*, 17(2):93–101.

Rüeger, J. (1992). *Electronic Distance Measurement: An Introduction*. Springer-Verlag.